Pharmacogn J. 2026; 18(2): 129-138
A Multifaceted Journal in the field of Natural Products and Pharmacognosy
www.phcogj.com

Original Article

Green-Synthesized Copper Nanoparticles from *Azadirachta Indica* for Antimicrobial Applications and Potential Visible-Light-Assisted Organic Load Reduction of POME

Anu Avudaiappan[1], Krittika Chandran[1], Sajna Keeyari Purayil[1], Abiramy Krishnan[1], Maimuna Gai[1], Aishath Aala Rasheed[1], Soh Lee May[1], Nur Izzah Bt Tohar[1], Jamal Moideen Muthu Mohamed[2]*

Anu Avudaiappan[1], Krittika Chandran[1], Sajna Keeyari Purayil[1], Abiramy Krishnan[1], Maimuna Gai[1], Aishath Aala Rasheed[1], Soh Lee May[1], Nur Izzah Bt Tohar[1], Jamal Moideen Muthu Mohamed[2]*

[1]Faculty of Pharmacy & BioMedical Sciences, MAHSA University, Bandar Saujana Putra, 42610 Jenjarom, Selangor, MALAYSIA.

[2]Department of Pharmacology, Faculty of Medicine, Manipal University College Malaysia, Jalan Batu Hampar, Bukit Baru, 75150 Melaka, MALAYSIA.

Correspondence

M. Jamal Moideen Muthu

Department of Pharmacology, Faculty of Medicine, Manipal University College Malaysia, Jalan Batu Hampar, Bukit Baru, 75150 Melaka, MALAYSIA

E-mail: jamal.mohamed@manipal.edu.my

History

- Submission Date: 18-02-2026;
- Review completed: 18-03-2026;
- Accepted Date: 30-03-2026.

DOI : 10.5530/pj.2026.18.126

Article Available online

http://www.phcogj.com/v18/i2

ABSTRACT

Objective: Palm Oil Mill Effluent (POME) is a high-strength agro-industrial wastewater of serious environmental concern due to its high organic load and microbial contamination. **Methods:** Copper nanoparticles (CuNPs) were synthesized using *Azadirachta indica* (neem) leaf extract and copper sulfate at different extract-to-metal salt ratios (1:1 and 2:1). The formation of CuNPs was confirmed by color change, FESEM, and EDX analyses. POME samples were collected from two treatment stages (raw and acidification ponds), and bacteria were isolated and identified using morphological, Gram staining, and biochemical tests. The antimicrobial activity of CuNPs at two concentrations (0.008 g and 0.016 g) was evaluated against isolated bacterial strains (*Bacillus* spp., *Pseudomonas* spp., and *Stenotrophomonas* spp.) using the agar well diffusion method. **Results:** The synthesized CuNPs ranged from 11–40 nm in size, confirming the presence of elemental copper with bioorganic capping. Antibacterial activity increased with CuNP loading, with the maximum inhibition zone (50 mm) observed for *Bacillus* spp. using CuNPs synthesized from a 0.1 M precursor solution and 0.016 g nanoparticle dose. At higher precursor concentrations (1.0 M), aggregation of nanoparticles occurred, leading to reduced antibacterial efficiency. Neem-CuNPs therefore demonstrated strong antimicrobial (disinfection) activity, while photocatalytic effects were observed as a secondary, light-assisted reduction of organic content rather than direct biodegradation. **Conclusion:** The green-synthesized CuNPs offer an eco-friendly and effective antimicrobial strategy for managing POME-associated bacteria. These findings provide a basis for future work combining CuNPs with biological systems to enhance wastewater remediation.

Keywords: Antimicrobial activity, Copper nanoparticles, *Azadirachta indica*, Disinfection, Green synthesis, Wastewater treatment

INTRODUCTION

The palm oil industry is one of the fastest-growing agro-industrial sectors, especially in Malaysia, Indonesia, Africa, and South America. It contributes significantly to national economies through exports and job creation, but also generates substantial waste, particularly palm oil mill effluent (POME). POME, a liquid by-product from crude palm oil extraction, arises from sterilization, clarification, and hydrocyclone separation stages[1]. It is a thick, brownish effluent with high discharge temperatures (often >80 °C) and extremely high organic loads, with COD levels exceeding 50,000 mg/L, making it far more polluting than domestic wastewater. If untreated, POME depletes dissolved oxygen in aquatic systems, causing hypoxia, eutrophication, and biodiversity loss[2,3]. Open anaerobic lagoons release methane (CH_4), intensifying climate change concerns, while residual oils, phenolics, heavy metals, and suspended solids threaten soil, groundwater, and public health in rural communities[4].

Although environmental laws exist, many mills lack modern treatment facilities due to cost and infrastructure limitations. Conventional systems like anaerobic ponds are land-intensive, slow, and often ineffective, sometimes leading to illegal discharges[5]. Therefore, there is an urgent need for sustainable and cost-effective alternatives. Advances in biotechnology, particularly bioremediation and nanotechnology, provide promising solutions. These strategies aim to reduce pollutant load of POME while enabling resource recovery and value-added products[6].

Photocatalysis has emerged as a ccomplementary treatment approach for the reduction of organic pollutants in wastewater, while antimicrobial disinfection remains essential for controlling pathogenic microbial loads. Metal nanoparticles, especially those synthesized from plant extracts, influence antimicrobial disinfection and light-assisted redox processes, depending on experimental conditions[7]. Copper nanoparticles (CuNPs) synthesized using *Azadirachta indica* (neem) leaf extract are particularly promising due to their redox activity, surface plasmon resonance, and antimicrobial properties. Compared with silver (Ag), zinc oxide (ZnO), titanium dioxide (TiO_2), and iron (Fe) nanoparticles, neem-mediated CuNPs often show competitive or superior antibacterial activity for POME. previous studies such as Niharika and Devra (2018) mainly focused on the synthesis and physicochemical characterization of neem-mediated CuNPs, their direct application to POME treatment remains underexplored[8].

Cite this article: Anu A, Krittika C, Sajna K P, Abiramy K, Maimuna G, Aishath A R, Soh L M, Nur I B T, Jamal M M M. Green-Synthesized Copper Nanoparticles from *Azadirachta Indica* for Antimicrobial Applications and Potential Visible-Light-Assisted Organic Load Reduction of POME. Pharmacogn J. 2026;18 (2): 129-138.

Unlike conventional chemical nanoparticle synthesis, which uses hazardous reducing agents, green synthesis with plant extracts provides a safe, sustainable, and scalable alternative. Neem leaves contain phytochemicals such as nimbin, quercetin, and azadirachtin, which act as reducing and capping agents[9].

Beyond photocatalysis, CuNPs can work synergistically with microbial consortia in biodegradation. Nanoparticles enhance enzyme production, electron transfer, and microbial metabolism, thereby creating effective bio-nano hybrid systems for complex effluents like POME[10]. Their integration with anaerobic digestion can also boost methane production while reducing inhibitory compounds such as long-chain fatty acids.

This study explores a sustainable nanobiotechnological strategy for POME treatment using CuNPs synthesized from *A. indica* leaves. These nanoparticles demonstrate antimicrobial effects useful for isolating and enriching POME-derived bacterial strains while also supporting biodegradation. By combining biosynthesized CuNPs with indigenous microbial consortia, we aim to establish a synergistic bio-nano platform for enhanced treatment of POME. This work contributes to scalable, eco-friendly wastewater management approaches, addressing both environmental and resource challenges in palm oil-producing regions.

MATERIALS AND METHODS

Materials

Fresh leaves of *Azadirachta indica* (neem) were collected from the vicinity of the main building at MAHSA University, Bandar Saujana Putra, Malaysia (2.9346° N, 101.5700° E). The botanical identity of the specimen was confirmed by a taxonomist at the Department of Biology, Universiti Putra Malaysia. A voucher specimen (Voucher No.: UPM 6892) was deposited in the university herbarium for future reference. Copper(II) sulfate pentahydrate ($CuSO_4{\cdot}5H_2O$) of 98% purity was procured from Chemiz (M) Sdn. Bhd. Selangor, Malaysia. Culture media of nutrient agar, oil agar (palm oil agar (POA)), Mineral Salt Medium (MSM), carboxymethyl cellulose (CMC) agar, tryptone brot, MR-VP mediu, simmon's citrate agar, pepton, TSI Aga, Urea, hydrogen peroxide, oxidase paper, Kovac's Reagent, Methyl Red solution, alpha-naphthol solution (VP1), Potassium peroxide (KOH) (VP2) purchased from HiMedia Laboratories, Maharashtra, India. MacConkey Agar (MAC), Gram stain set, 250 mL of Crystal violet, Iodine, Decolorizer, Safranin procured from Thermo Fisher Scientific Malaysia Sdn. Bhd. Penang, Malaysia.

Synthesis of CuNPs

The leaves were washed, chopped, and boiled with water (10 g leaves in 100 mL of distilled water) at 90 °C for 2 h to extract phytochemicals. The extract was filtered to obtain a clear greenish-brown solution. Copper(II) sulfate pentahydrate ($CuSO_4{\cdot}5H_2O$) stock solutions were prepared at three molarities are 0.1 M (2.49 g in 100 mL distilled water), 0.5 M (12.46 g in 100 mL), and 1.0 M (24.93 g in 100 mL). For nanoparticle synthesis, the neem extract was mixed with copper sulfate ($CuSO_4{\cdot}5H_2O$) solutions at two different ratios: 1:1 and 2:1 (extract: metal salt solution). The mixtures were heated again at 90 °C for 2 h with continuous stirring. A visible colour changes from blue to brownish-black indicated CuNP formation[11]. The mixtures were left overnight to stabilise followed by centrifugation at 6000 rpm for 10 min, washing and drying at 70°C overnight to obtain brown CuNP.

Following centrifugation and reaction completion, the CuNP precipitate was collected, purified, and oven-dried at 60 °C until a uniform weight was achieved. The actual yield (0.8 $mg{\cdot}mL^{-1}$ and 1.6 $mg{\cdot}mL^{-1}$ from 10 mL reactions at 0.5 M and 1.0 M precursor, respectively) of the dried CuNPs was measured by weight. The CuNP powder was reconstituted in sterile distilled water and ultrasonically agitated to create working suspensions with specified concentrations (measured in mg/mL) for biological tests. For instance, 0.8 mg/mL was equivalent to 0.8 $mg{\cdot}mL^{-1}$ g of CuNPs reconstituted in 10 mL of water. Instead of using the precursor molarity, these standardized solutions were used for all antibacterial and photocatalytic studies.

Field-Emission Scanning Electron Microscopy (FESEM) ofCuNPs

The prepared surface structure and morphology of CuNPs were examined using a Field-Emission Scanning Electron Microscope (FESEM; SUPRA 55VP, Carl Zeiss, Germany). Using double-sided carbon tape attached to an aluminum stub, 1 mg of the dried CuNP powder was evenly distributed. To avoid charge and improve picture quality, the samples were then sputter-coated with a thin coating of platinum (about 5 nm thick) using a Quorum SC7620 sputter coater. In order to observe particle size and surface shape, micrographs were taken at various magnifications under high vacuum and at an accelerating voltage of 5–15 kV[12].

Energy-dispersive X-ray (EDX) analysis of CuNPs

A standard EDX spectrometer connected to the FESEM device was used to ascertain the chemical composition and purity of the produced CuNPs. The spectra, which were obtained in the 0–20 keV energy range, verified the existence of distinctive oxygen (O) and copper (Cu) peaks devoid of any impurity signals[13]. To ensure compositional uniformity, quantitative analysis was used to estimate the relative atomic percentages of Cu and O for samples made from varying precursor concentrations.

Collection and Storage of Raw Palm Oil Mill Effluent (POME)

POME samples were collected from Seri Bandar Palm Oil Mill in Malaysia at two treatment stages, namely the raw pond (Pond 1) and the acidification pond (Pond 2). Within 4 h after collection, each sample was taken in sterile 500 mL amber glass bottles, carefully sealed, and brought to the lab. To maintain sample integrity, samples were used for all experimental analyses within 48 h of collection and kept in the dark at 4 °C to avoid microbial overgrowth and compositional alterations[14].

Photocatalytic Degradation Assay (PDA)

This assay was conducted to preliminarily evaluate the light-assisted organic load reduction potential of CuNPs. It was designed independently from antibacterial assays and does not assess microbial inactivation. The light-assisted photocatalytic activity of CuNPs toward organic content reduction in POME was preliminarily evaluated using palm oil mill effluent (POME) as a model organic matrix. For the assay, 100 mL of raw POME (pH 6.8) was mixed with CuNPs (1.0 mg/mL) and magnetically stirred under visible light illumination (LED lamp, 60 W, λ = 420–700 nm, 5000 lux) at ambient temperature. The mixture was maintained under constant aeration to ensure uniform dispersion and oxygen supply[15]. A dark control (POME + CuNPs without light) and a light-only control (POME without CuNPs) were simultaneously run. Samples (5 mL) were collected at 0, 30, 60, and 90 min, centrifuged (10,000 rpm, 10 min), and analyzed for total organic carbon (TOC) reduction using a TOC analyzer (Shimadzu TOC-L). The degradation efficiency (%) was calculated as:

$$Degradation\,(\%) = \frac{Co - Ct}{Co} \times 100$$

Where C_0 and C_t are TOC value at initial and time t, respectively.

Preparation of Nutrient Agar

Medium was prepared following the manufacturer's protocol (OXOID). Approximately 28 g of the nutrient agar was dissolved in 1000 mL of distilled water, boiled to dissolve completely, followed by autoclaving at 121°C for a duration of 15 min. After autoclaving, the media was poured into a sterile petri dish, around 20 mL for each plate. The plates were stored at 4°C.

Preparation of MSM-POA Medium

The POA was prepared by dissolving 2.78 g of mineral salt agar in accordance with the manufacturer's protocol (HiMedia) in 100 mL of distilled water with constant stirring, followed by sterilization at 121°C for 15 min. Once cooled to around 50 °C, 3.12 g of filtered palm oil was added and thoroughly mixed to ensure even distribution throughout the medium. The final mixture was poured into sterile petri dishes under aseptic conditions. The plates were stored at 4°C.

Preparation of MAC Agar

MAC agar is a selective medium used to differentiate gram-negative bacteria based on lactose fermentation. Medium was prepared following the manufacturer's protocol (HiMedia). Approximately 49.53 g of the mineral salt agar was dissolved in 1000 mL of distilled water, boiled to dissolve completely, and then autoclaved at 121 °C for a duration of 15 min[16]. After autoclaving, the media was poured into a sterile petri dish, around 20 mL for each plate.

Evaluation of Antibacterial Activity

Nutrient agar plates were prepared and sterilized, and then spread the POME sample (Pond 1 and 2). Small wells were made in the agar, and synthesis ratios of CuNPs (1:1 and 2:1) in different concentrations (0.8 $mg{\cdot}mL^{-1}$ and 1.6 $mg{\cdot}mL^{-1}$) were added. The plates were incubated at 37 ± 0.5°C for 24 to 48 h[17]. Clear zones around the wells showed where bacteria were killed or inhibited. Larger zones meant more effective antibacterial action.

Bacterial Isolation and Identification

For bacterial isolation, the serial dilution method was used. The POME sample was diluted stepwise up to 10^{-7}, and selected dilutions (10^{-3}, 10^{-5}, 10^{-7}) were spread onto the prepared agar plate, followed by incubation at 37± 0.5 °C for 24 h. Distinct colonies were isolated using the quadrant streak method to obtain pure cultures. The purified colonies were observed and documented for their morphological traits such as shape, colour, size, surface texture, and elevation[18]. Gram staining was performed to identify the Gram-positive and Gram-negative bacteria based on their cell wall structure. The isolates were stored on agar slants at 4°C for further analysis. The isolates were identified based on their morphological and biochemical characteristics. These findings offer a presumptive genus-level identification; molecular methods like 16S rRNA sequencing would be necessary for a definitive species identification, which was outside the purview of this investigation.

Bacterial Inhibition Testing

Two complimentary techniques were used to evaluate antibacterial activities of CuNPs are direct plating of POME samples and agar well diffusion against reference strains. POME plating involved serially diluting 100 µL of POME wastewater (10^{-1}–10^{-6}) in sterile saline, then spreading 100 µL aliquots of each dilution onto nutrient agar plates. Bacterial cultures were grown in nutrient broth until reaching the logarithmic growth phase, defined by an optical density of OD_{600} = 0.4–0.6. Standardized inocula (10^8 CFU/mL) were spread evenly onto nutrient agar plates to form uniform bacterial lawns[19]. Colonies were enumerated after being incubated for 24 hours at 37 °C (30–300 CFU/plate range). Well diffusion assay involves the *P. aeruginosa* and *Bacillus cereus* overnight cultures were uniformly distributed across Mueller-Hinton agar plates after being adjusted to 0.5 McFarland standard (~1×10^8 CFU/mL). 50 µL of CuNP suspensions at certain concentrations (0.8 mg/mL and 1.6 mg/mL, made by redistributing dry CuNPs) were added to each well after wells (6 mm in dm) had been punched. The control wells contained gentamicin (10 µg/mL) as a positive antibiotic control; neem extract only (plant extract control), and sterile distilled water (negative control). Inhibition zones were measured in millimeters after plates were incubated at 37 ± 0.5 °C for 24 h. Three duplicates of each assay were run, and mean ZOI ± SD were determined.

Statistical analysis

The results are shown as mean ± standard deviation (SD), and each experiment was run in triplicate. Tukey's post hoc test (GraphPad Prism 9.0) was used after a one-way ANOVA to examine statistical differences between groups. p-values < 0.05 were regarded as statistically significant. Throughout the manuscript, precursor concentration (M) refers exclusively to the molarity of $CuSO_4{\cdot}5H_2O$ used during synthesis, whereas all experimental concentrations of CuNPs in suspension are reported as $mg{\cdot}mL^{-1}$ based on the dry nanoparticle mass.

RESULTS AND DISCUSSION

Morphology

FESEM was used to examine the surface morphology and particle size distribution of the photocatalysts and Cu dopant dispersion within the nanoparticles (Figure 1). The images reveal mostly spherical to irregular CuNPs with different extents of agglomeration, the typical feature owing to high surface energy and the tendency of nanoparticles to agglomerate. The nanoscale dimensions from the chosen measurement regions range from about 11.17 nm to 40.99 nm across the three images. The biggest particle size that was measured was ~40.99 nm, and the smallest was ~11.17 nm, indicating successful synthesis of nanoparticles with a size in the nanometer range. The products were in the nanoparticle range, with average diameters of 24.97–40.99 nm for 0.1 M Cu (Figure 1a), 13.44–15.19 nm for 0.5 M Cu (Figure 1b), and 11.17–12.33 nm for 1.0 M Cu (Figure 1c). CuNPs synthesized with 0.1 M copper were larger and more aggregated, while those from 0.5 M were smaller and more defined. The 1.0 M sample yielded the smallest and most uniformly dispersed nanoparticles.

The precursor molarity (0.1–1.0 M) influenced both the yield and particle size distribution of the synthesized CuNPs. Increasing $CuSO_4$ concentration from 0.1 M to 1.0 M raised the nanoparticle yield (from 0.3 to 1.6 $mg{\cdot}mL^{-1}$ g/10 mL batch), producing more concentrated suspensions (0.3–1.6 mg/mL). These standardized suspensions were used for dose-dependent antibacterial assays and photocatalytic degradation studies, ensuring reproducibility. Size differences between images can be attributed to different nucleation and growth rates during synthesis and potential aggregation effects. The relatively regular positioning of finer particles in later images indicates high yields of fine nanoparticles, and bigger particles within the initial image may be indicative of aggregated morphology or nuclei overgrowth[20]. Overall, FESEM confirm that particle size decreases with increasing precursor molarity due to rapid nucleation and limited growth at higher Cu^{2+} concentrations, consistent with classical nucleation theory.

Elemental composition of CuNPs

The effective synthesis of CuNPs with bio-organic capping was demonstrated by the EDX spectra, which verified the presence of copper (Cu) and oxygen (O) as the main constituents. With very few impurity signals, the distinctive Cu peaks (about 0.9 keV and 8.0

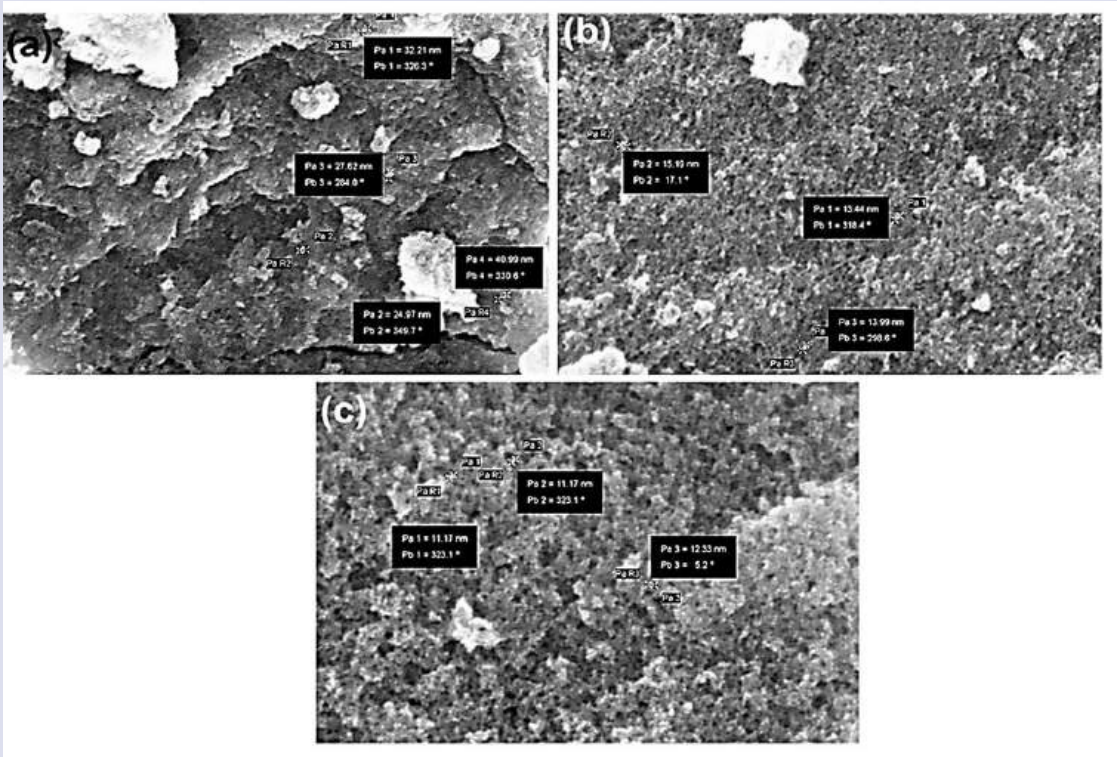

Figure 1. FESEM images of CuNPs synthesized from $CuSO_4$ precursor solutions at (a) 0.1 M, (b) 0.5 M, and (c) 1.0 M. Scale bars = 100 nm. Particle size distribution was measured from 100 individual nanoparticles per sample using ImageJ software. Mean particle diameters are shown on each subfigure.

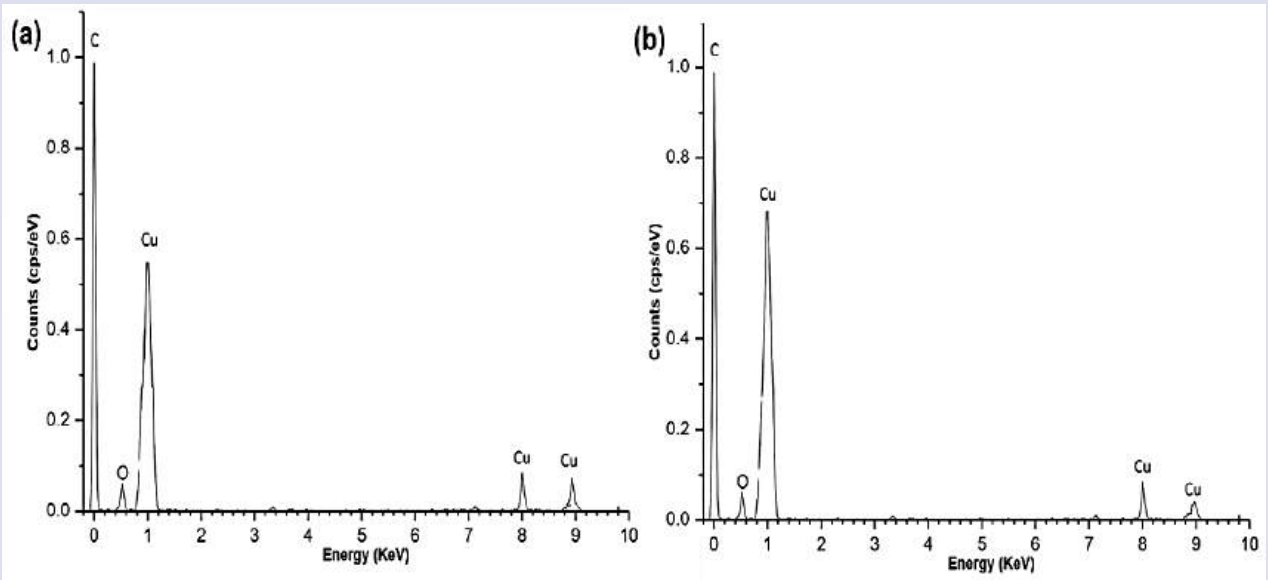

Figure 2.EDX spectra of green-synthesized CuNPs from *A. indica* leaf extract using precursor concentrations of (a) 0.1 M and (b) 1.0 M $CuSO_4{\cdot}5H_2O$. Prominent peaks corresponding to Cu (Kα, Lα) and O (Kα) confirm the presence of elemental copper with surface oxide or bioorganic capping. The Cu/O ratio increases with precursor concentration, indicating enhanced metal purity and nanoparticle formation efficiency.

keV) and O peaks (about 0.5 keV) were reliably seen in all samples. The Prepared CuNPs exceptional elemental purity and stability were indicated by a quantitative evaluation of the Cu/O ratios. The patterns in particle size distribution are therefore based on FESEM observations rather than EDX interpretation, although the EDX results confirm elemental composition[21]. Table 1 highlights that increasing precursor concentration increases Cu content and purity of the prepared CuNPs. According to Nguyen et al. (2014), higher precursor concentrations accelerate nucleation, leading to rapid formation of smaller particles, whereas slower nucleation at lower concentrations allows for larger particle growth. Thus, CuNPs synthesized from 1.0 M copper precursor exhibited smaller particle sizes with more uniform dispersion compared to those synthesized from 0.1 M precursor, which produced larger, more aggregated particles[22,23] (Figure 2).

PDA

Using the 1.0 M precursor-derived CuNPs, the CuNPs showed visible-light-driven photocatalytic activity, removing 91.8% of the TOC in 90 minutes as opposed to 77.6% for 0.5 M and 58.3% for 0.1 M formulations. The dark or light-only controls showed very little degradation (<10%), indicating that photocatalysis was the responsible for organic content reduction, while antibacterial effects were evaluated separately and are not attributed to this assay. There was a substantial difference between the treatments, according to statistical analysis (ANOVA, $p < 0.001$), with 1.0 CuNPs synthesized from a 1.0 M $CuSO_4 \cdot 5H_2O$ precursor solution exhibiting the maximum activity. The increased surface plasmon resonance and smaller crystallite size of the CuNPs, which encourage charge separation and the production of reactive oxygen species (ROS) in the presence of light, are responsible for the improved degrading efficiency. CuNPs absorb photons under visible light, producing electron–hole pairs ($Cu^0 \rightarrow Cu^+ + e^-$). Superoxide ($\bullet O_2^-$) and hydroxyl ($\bullet OH$) radicals are formed when these charge carriers combine with oxygen and water, oxidizing organic contaminants in POME to CO_2 and H_2O[24] (Figure 3).

Grams Staining

The microscopic analysis of the isolated bacterial strains revealed rod-shaped cells, often appearing singly or in pairs (Figure 4a). Gram staining showed that one isolate was Gram-positive, retaining the crystal violet stain and appearing purple, indicative of a thick peptidoglycan cell wall (Figure 4a). The presence of unstained, elliptical endospores further confirmed it as a spore-forming bacterium, consistent with the *Bacillus* genus[25]. A second isolate, presumptively identified as *Stenotrophomonas maltophilia*, exhibited Gram-negative, rod-shaped morphology (Figure 4b). Another isolate, designated Bacteria 2, formed well-isolated colonies with greenish pigmentation on nutrient agar, suggesting its identity as *Pseudomonas aeruginosa* (Figure 4c) and Gram staining confirmed it as Gram-negative.

Biochemical and Functional Characterization

Biochemical characterization of bacterial strains isolated from POME (Table 2) indicated profiles consistent with *Bacillus*, *Pseudomonas*, and *Stenotrophomonas* genera. While the observed patterns are suggestive of *B. subtilis*, *P. aeruginosa*, and *S. maltophilia*, these identifications remain presumptive, as molecular confirmation (e.g., 16S rRNA sequencing) was not performed[26]. Another isolate designated Bacteria 2, formed well-isolated colonies with greenish pigmentation on nutrient agar, suggesting its identity as *P. aeruginosa*. Gram staining confirmed it as Gram-negative, and its biochemical profile aligned with *Pseudomonas* characteristics negative for MR, VP, indole, and urease, but positive for citrate, catalase, and oxidase activity. The strain did not ferment sugars in the TSI test, confirming its oxidative metabolism based on the Abdelaziz et al. (2023) outcome[27].

Based on biochemical profiles, species-level identification is expected for *B. subtilis, P. aeruginosa, and S. maltophilia.* Molecular identification, such as 16S rRNA gene sequencing, would be necessary for confirmation.

The biochemical overview was followed by the interpretation of strain-specific characteristics. *B. subtilis* demonstrated aerobic metabolism and the capacity to use a variety of carbon sources, which are characteristics consistent with its environmental adaptability, as demonstrated by positive results for the catalase, oxidase, citrate, and Voges-Proskauer tests. *P. aeruginosa* demonstrated its capacity to produce biosurfactants and oxidative metabolism by forming greenish-pigmented colonies on nutrient agar and testing positive for catalase, oxidase, and citrate consumption[28]. The decomposition of palm oil in POME settings was facilitated by lipid hydrolysis, which is suggested by the presence of extracellular lipase activity. Strong metabolic flexibility was demonstrated by the third isolate, *S.maltophilia*, which tested positive for catalase, oxidase, urease, and citrate utilization. The emulsification zones seen during growth on MSM-POA medium point to the solubilization of palm oil constituents by biosurfactants[29]. When

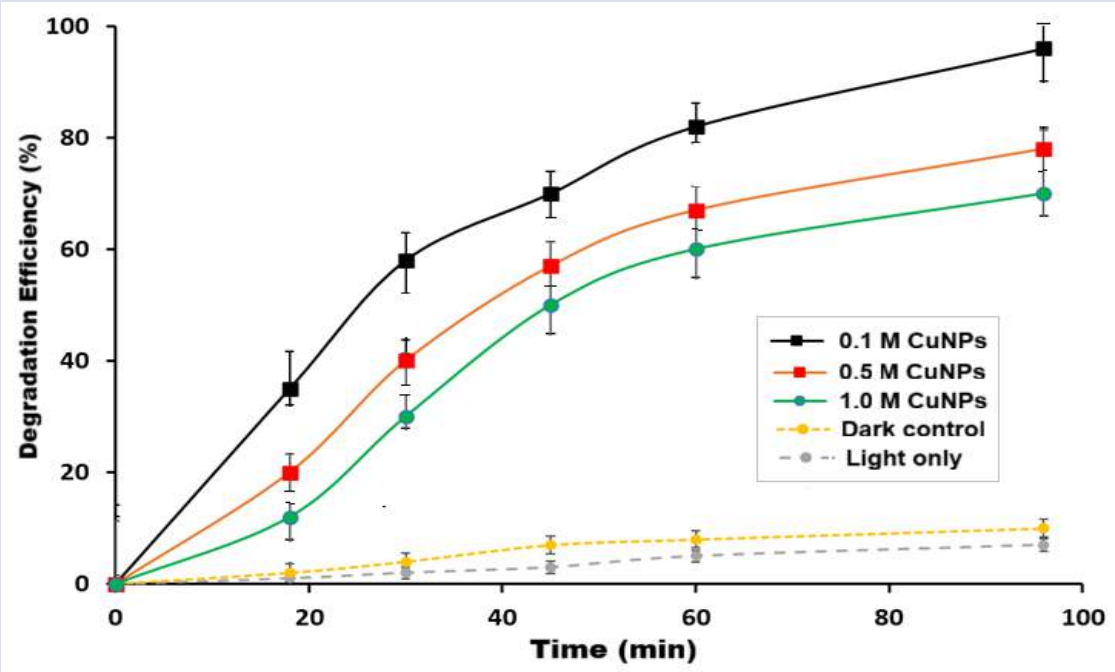

Figure 3. Visible-light-assisted reduction of organic content (TOC) in POME using CuNPs synthesized from different precursor concentrations (0.1 M, 0.5 M, and 1.0 M). Results expressed as mean ± SD (n = 3).

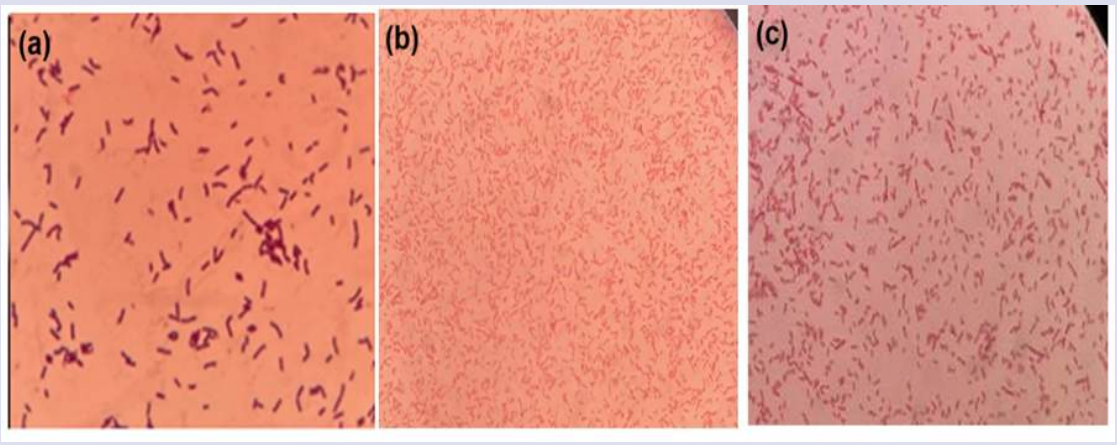

Figure 4. The Gram staining performance observed under a light microscope for (a) *Bacillus,* (b) *Pseudomonas*, (c) *Stenotrophomonas maltophilia*

Table 1. The atomic (%) and weight (%) composition for each element (Cu, O, C).

Sample	Cu (wt%)	O (wt%)	C (wt%)	Cu/O Ratio
0.1 M CuNPs	68.4	23.5	8.1	2.91
1.0 M CuNPs	78.9	17.2	3.9	4.58

Table 2. Biochemical test results of bacterial isolates from POME showing presumptive identification based on morphological and biochemical characteristics

Biochemical Test	Results		
	B. subtilis	P.aeruginosa	S.maltophilia
Methyl Red (MR) Test	–	–	–
Voges-Proskauer (VP) Test	+	–	–
Citrate Test	+	+	+
Urease Test	–	–	+
Catalase Test	+	+	+
Oxidase Test	+	+	+
Triple Sugar Iron (TSI) test	–	–	–

Note: (+) indicates a positive reaction; (–) indicates a negative reaction. POME – Palm Oil Mill Effluent; *B. subtilis* – *Bacillus subtilis*; *P. aeruginosa* – *Pseudomonas aeruginosa*; *S. maltophilia* – *Stenotrophomonas maltophilia*

taken as a whole, these biochemical characteristics demonstrate how Pseudomonas and Stenotrophomonas contribute to the generation of biosurfactants and the breakdown of lipids, two important processes in POME remediation.

Growth on MacConkey agar produced pale, translucent colonies, consistent with non-lactose fermentation, and the light green hue suggested pyocyanin production, a virulence factor and redox-active compound. On MSA, the colonies appeared irregular, mucoid, and slightly translucent, with zones of clearing, indicating extracellular enzyme activity, likely lipase-mediated, these features suggest biosurfactant and lipase production, facilitating palm oil degradation. A third isolate, presumptively identified as *Stenotrophomonas maltophilia*, exhibited Gram-negative, rod-shaped morphology and a biochemical profile marked by positive reactions for citrate, urease, catalase, and oxidase, but negative for MR and VP tests.

Its metabolic flexibility is well-documented in environmental adaptation. When grown on MSM-POA, initial growth was delayed, but visible colonies formed after 48 h, accompanied by white emulsification zones, this concept suggesting biosurfactant-mediated solubilization of palm oil in accordance with the Williams et al. 2025[30]. Unlike *Bacillus*, which did not produce clear hydrolytic zones, *Stenotrophomonas* appeared to utilize emulsification rather than enzymatic hydrolysis, consistent with biosurfactant-assisted degradation mechanisms (Figure 5a and b). Together, these observations shown in Figure 5c and d, confirm the potential of *Pseudomonas aeruginosa* and *Stenotrophomonas maltophilia* in the bioremediation of POME through a combination of biosurfactant production, oxidative metabolism, and selective hydrocarbon degradation pathways, which is consistent with Thomas et al. 2014 outcome[31].

Antibacterial Effect of CuNPs against POME-Associated Bacteria

Bacillus spp.

Neem-synthesized CuNPs exhibited strong antibacterial activity against *Bacillus spp*., a Gram-positive bacterium commonly present in POME. As shown in Figure 5a, the combination of 0.1 M precursor and 1.6 $mg{\cdot}mL^{-1}$ CuNP loading (1:1 ratio) produced the largest inhibition zone (50 mm) against *Bacillus cereus*, followed by 0.5 M (42 mm) and 1.0 M (35 mm). The investigation considered varying copper precursor concentrations (0.1 M, 0.5 M, 1.0 M), nanoparticle weights (0.8 $mg{\cdot}mL^{-1}$, 1.6 $mg{\cdot}mL^{-1}$), and synthesis ratios of plant extract to metal salt (1:1 and 2:1). At a 1:1 synthesis ratio, the 0.1 M copper concentration combined with 1.6 $mg{\cdot}mL^{-1}$ of CuNPs yielded the largest inhibition zone (50 mm), suggesting optimal nanoparticle stability and dispersion. In contrast, higher copper concentrations (0.5 M and 1.0 M) at the same nanoparticle weight produced reduced inhibition zones of 40 mm and 35 mm, respectively (Figure 6a). This trend likely reflects nanoparticle agglomeration at higher metal concentrations, according to Todorova et al. 2025, which reduces active surface area and antimicrobial efficacy[32].

At the 2:1 synthesis ratio, where neem extract was in excess, the highest inhibition (42 mm) was observed at 0.5 M with 1.6 $mg{\cdot}mL^{-1}$ CuNPs. Although neem phytochemicals aid in capping and stabilization, an overabundance may hinder Cu^{2+} ion release, slightly diminishing antibacterial potency compared to the 1:1 ratio. Across both synthesis ratios, increasing the nanoparticle weight consistently improved antibacterial outcomes, reinforcing the role of CuNPs loading in enhancing contact with bacterial cells based on Ifijen et al. 2025[33].

Surface oxidation of CuNPs in aqueous and aerobic environments encourages the production of ROS, including hydrogen peroxide (H_2O_2), superoxide anions ($O_2{\bullet}^-$), and hydroxyl radicals (•OH). Essential macromolecules including proteins, lipids, and DNA are harmed by the oxidative stress that these extremely reactive species

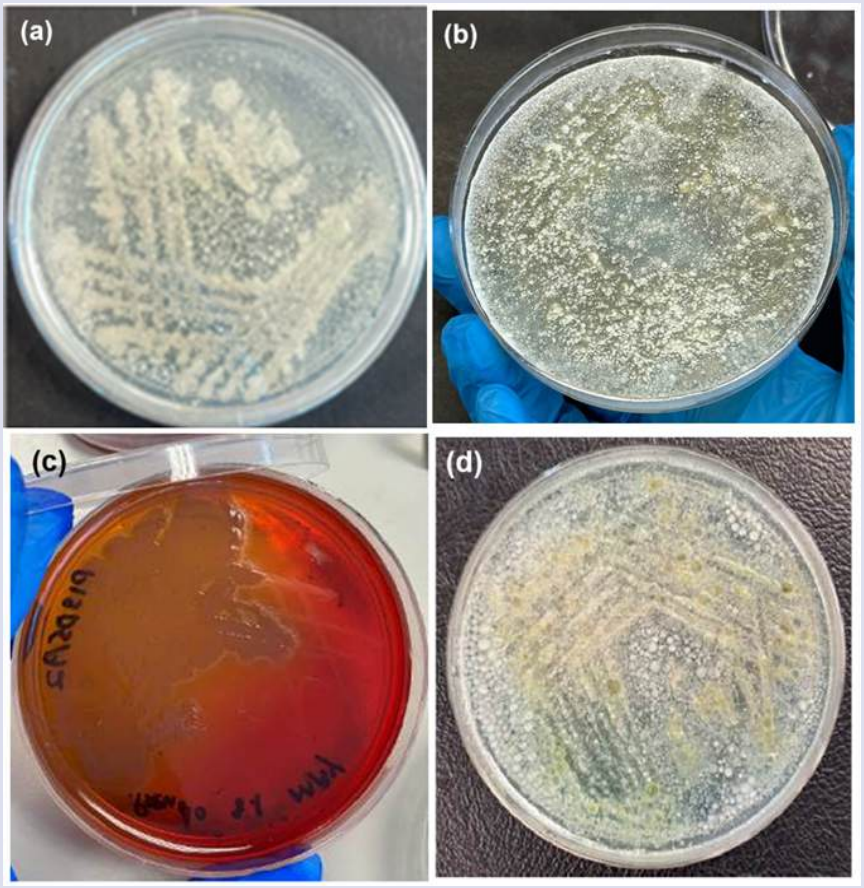

Figure 5. Isolated pure colonies streaked on MSM-POA of (a) *Bacillus* sp. (b) *Stenotrophomonas sp*. The colony growth and pigmentation of *Pseudomonas*on MSM-POA(c) and (d)*Bacillus sp* on MAC

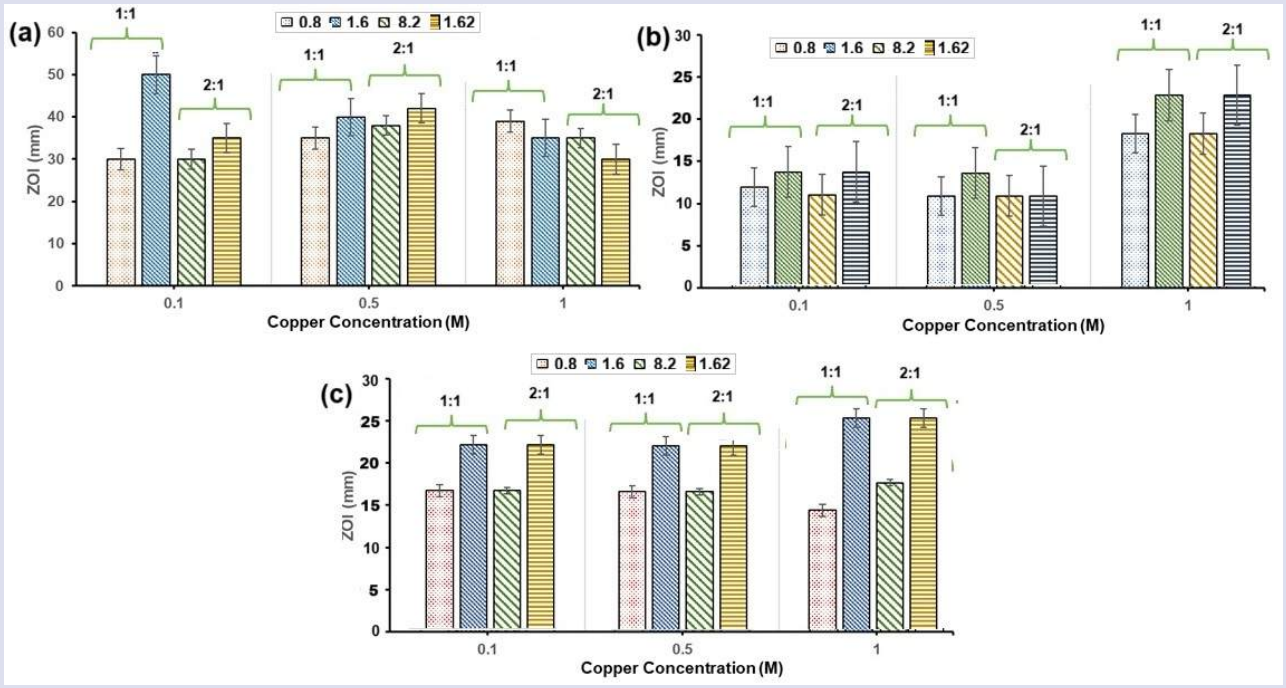

Figure 6. Antimicrobial activity of (a) *Bacillus sp*., of CuNPs synthesized from varying precursor concentrations (0.1 M, 0.5 M, 1.0 M) and CuNP loadings (0.8 mg·mL^{-1}, 1.6 mg·mL^{-1}). Maximum inhibition (50 mm) observed for 0.1 CuNPs synthesized from a 1.0 M $CuSO_4{\cdot}5H_2O$ precursor solution at 1.6 mg·mL^{-1} loading (1:1 ratio). (b) *Pseudomonass sp*., and (c) *Stenotrophomonass sp*. against POME-associated pathogens in the presence of CuNPs. Mean ± SD (n = 3).

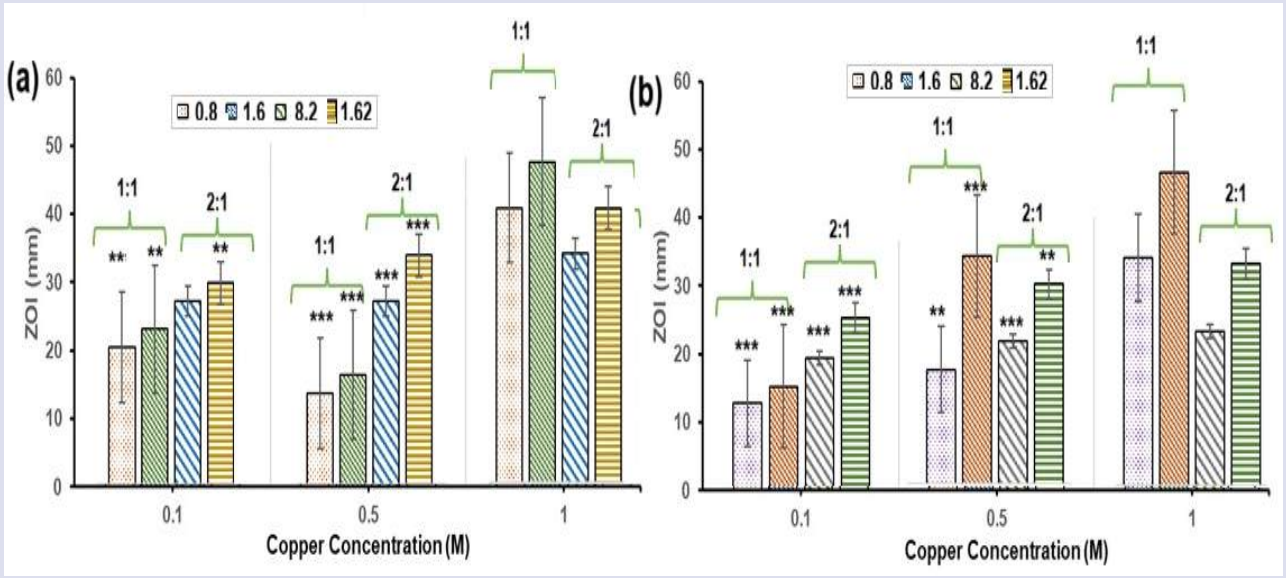

Figure 7. Antibacterial activity of CuNPs synthesized using different extract-to-precursor ratios against bacteria from POME (Pond 1 and Pond 2). Data shown as mean ± SD (n=3). Statistical analysis performed using one-way ANOVA, $p < 0.05$.

cause in bacterial cells (Mammari et al., 2022). At the same time, released Cu^{2+} ions interact with the negatively charged bacterial cell wall, causing permeability to increase and membrane integrity to be disrupted. Cell death eventually follows from cytoplasmic leakage[34,35].

Pseudomonas spp.

Pseudomonas spp., known for their intrinsic resistance to antimicrobial agents, exhibited relatively weak inhibition at lower CuNP concentrations. At both 0.1 M and 0.5 M, inhibition zones remained modest (12–15 mm), regardless of nanoparticle mass or synthesis ratio (Figure 6b). This limited effect is attributed to the robust defense mechanisms of *Pseudomonas*, including low outer membrane permeability, metal-efflux systems (e.g., CzcCBA), and ROS-neutralizing enzymes based on Elfadadny et al. 2024 research work[36]. A significant improvement was observed at 1.0 M copper concentration. At this level, inhibition zones expanded to 20 mm (0.8 mg·mL^{-1}) and 25 mm (1.6 mg·mL^{-1}), indicating that elevated copper levels are necessary to overcome theresistanceof bacterium. This effect, due to higher Cu^{2+} availability, likely boosts ROS generation and membrane interaction, overwhelming efflux systems and causing oxidative damage[37].

The results affirm that while nanoparticle dosage contributes to antibacterial performance, copper concentration is the critical factor when targeting highly resistant Gram-negative species like *Pseudomonas*. This highlights the importance of tailoring nanoparticle formulations to match the resistance profiles of target pathogens.

Stenotrophomonas maltophilia

Stenotrophomonas maltophilia, another Gram-negative opportunistic pathogen commonly found in POME, displayed moderate sensitivity to neem-synthesized CuNPs. The most pronounced inhibition was observed at 1.0 M copper with 1.6 mg·mL^{-1} of nanoparticles, yielding a zone of 23 mm. At lower nanoparticle weights (0.8 mg·mL^{-1}), inhibition was reduced (13–16 mm), underscoring the combined importance of high copper concentration and sufficient nanoparticle mass (Figure 6c).

The resistance of S. maltophilia stems from its ability to form biofilms, utilize metal efflux pumps (e.g. SmeDEF), and produce metal-binding proteins. Nevertheless, high concentrations of CuNPs appear to disrupt these defenses by inducing oxidative stress and destabilizing the outer membrane. The generation of ROS and release of Cu^{2+} ions contribute to protein denaturation, lipid peroxidation, and DNA damage, consistent with previously reported mechanisms by Brooke 2021[38]. These findings suggest that neem-mediated CuNPs can be tuned to effectively inhibit S. maltophilia by optimizing synthesis conditions, particularly copper precursor concentration and nanoparticle loading.

Antibacterial Effect of CuNPs against POME in Pond 1 and Pond 2

POME plating revealed a microbial load of ~1.2 × 10^5 CFU/mL, dominated by *Bacillus* and *Pseudomonas* species, confirming the wastewater as a natural microbial source[39]. In the well diffusion assay, CuNPs were dose-dependent, with 1.6 mg/mL CuNPs producing significantly larger zones (18.2 ± 0.8 mm against *B. cereus*, 15.6 ± 0.7 mm against *P. aeruginosa*) compared to 0.8 mg·mL^{-1} suspensions (12.5 ± 0.6 mm and 10.1 ± 0.5 mm, respectively). ANOVA confirmed significant differences between treatments ($p < 0.001$), and Tukey's test showed that both CuNP concentrations were significantly superior to controls ($p < 0.001$), while neem extract alone showed no inhibition ($p > 0.05$). Gentamicin showed the largest inhibition zone (~21 mm), which was statistically higher than CuNPs at 0.8 mg·mL^{-1} but not significantly different from CuNPs synthesized from a 1.0 M $CuSO_4{\cdot}5H_2O$ precursor solution at 1.6 mg/mL ($p > 0.05$). The 2:1 ratio also showed antibacterial activity, but slightly reduced, possibly due to excess phytochemicals hindering nanoparticle reactivity[39]. The 0.5 M concentration consistently exhibited the weakest antibacterial effect, as shown in Figure 7a. Overall, the study highlights the importance of optimizing synthesis conditions to enhance the antibacterial efficacy of synthesized CuNPs for potential use in environmental bioremediation[40].

The antibacterial evaluation of neem-mediated CuNPs using POME from Pond 2 showed that the 1:1 synthesis ratio (copper sulfate to neem extract) consistently produced larger inhibition zones than the 2:1 ratio. The highest antibacterial effect was observed at 1.0 CuNPs synthesized from a 1.0 M $CuSO_4{\cdot}5H_2O$ precursor solution with 1.6 mg·mL^{-1}g dosage in the 1:1 ratio, yielding a 55 mm inhibition zone. Even at lower concentrations, the 1:1 ratio maintained strong activity,

suggesting optimal nanoparticle formation and bioactivity[41]. In contrast, the 2:1 ratio, despite excess neem extract, showed slightly reduced effectiveness due to possible over-capping, which may limit Cu^{2+} ion release. Both ratios exhibited dose-dependent antibacterial action, but the 1:1 formulation proved superior and more consistent, as shown in Figure 7b. These findings highlight its potential for effective wastewater disinfection and environmental bioremediation, according to the conclusion revealed by Wylie et al. 2022[42].

Mechanistic Role of Photocatalysis

The enhanced antibacterial effects of CuNPs could also relate to photocatalytic-like mechanisms, as supported by prior literature on metal nanoparticles. While this study evaluated light-assisted organic load reduction using TOC analysis, photocatalytic mechanisms were not directly correlated with microbial inactivation. Therefore, antibacterial activity and photocatalytic organic degradation are discussed as distinct but potentially complementary processes. Future work should include quantitative photocatalytic assays (e.g., COD or dye degradation) to validate this hypothesis. Electrons reduce molecular oxygen to form superoxide radicals ($O_2^{-}\bullet$), while holes oxidize water to generate hydroxyl radicals (•OH), both of which possess strong antimicrobial potential. These ROS not only damage microbial cells but also play a role in degrading organic pollutants in POME, offering a dual-function benefit of disinfection and environmental remediation[43].

CONCLUSION

This study demonstrates the successful sustainable synthesis of copper nanoparticles (CuNPs) using *Azadirachta indica* leaf extract, offering an eco-friendly route for producing bioactive nanomaterials. The inverse relationship between precursor concentration and nanoparticle size yielded smaller, more reactive CuNPs at higher copper levels, enhancing their antimicrobial (disinfection) efficacy, while exhibiting secondary potential for light-assisted organic load reduction. The synthesized CuNPs exhibited strong antibacterial activity against both individual strains (notably *Bacillus*, *Pseudomonas aeruginosa*, and *Stenotrophomonas maltophilia*) and complex microbial communities in POME, with optimal performance at a balanced 1:1 CuNP-to-sample ratio. These findings underscore the potential of neem-mediated CuNPs as a cost-effective and sustainable antibacterial disinfection agent for industrial wastewater treatment, with additional potential for photocatalytic enhancement. Future studies should focus on their long-term stability, environmental interactions, and scale-up potential for broader applications in environmental and biomedical fields.

ACKNOWLEDGMENT

The authors are grateful to the Faculty of Pharmacy &BioMedical Sciences, MAHSA University, Bandar Saujana Putra, 42610 Jenjarom, Selangor, Malaysia for providing necessary facilities to develop this research work.

REFERENCES

1. Murphy DJ, Goggin K, Paterson RRM. Oil palm in the 2020s and beyond: challenges and solutions. CABI Agric Biosci. 2021;2:39. https://doi.org/10.1186/s43170-021-00058-3
2. Bello MM, Nourouzi MM, Chuah Abdullah L, Thomas Choong SY, Koay YS and Keshani S. POME is treated for removal of color from biologically treated POME in a fixed bed column: Applying wavelet neural network (WNN). J Hazard Mater. 2013;262C:106-113. http://dx.doi.org/10.1016/j.jhazmat.2013.06.053
3. Low SS, Bong KX, Mubashir M, Cheng CK, Lam MK, Lim JW, Ho YC, Lee KT, Munawaroh HSH, Show PL. Microalgae Cultivation in Palm Oil Mill Effluent (POME) Treatment and Biofuel Production. Sustainability 2021;13(6):3247. http://dx.doi.org/10.3390/su13063247
4. Yacob S, Ali Hassan M, Shirai Y, Wakisaka M, Subash S. Baseline study of methane emission from anaerobic ponds of palm oil mill effluent treatment. Sci Total Environ. 2006;366(1):187-96.
5. Mohd Hanafiah K, Abd Mutalib AH, Miard P, Goh CS, Mohd Sah SA, Ruppert N. Impact of Malaysian palm oil on sustainable development goals: co-benefits and trade-offs across mitigation strategies. Sustain Sci. 2022;17(4):1639-1661. http://dx.doi.org/10.1007/s11625-021-01052-4
6. Florindo Guedes MI, Tramontina FE, Lima F, Benjamin RS. Current trends in nanotechnology for bioremediation. Intern J. Environ. Pollut. 2020;1. http://dx.doi.org/10.1504/IJEP.2019.104526
7. Hansamali P, Evyan CY and Zakaria S. A Short Review: Photocatalysis As An Alternative Method for POME Treatment. J Eng Technol Appl Phys. 2024;6:32-39. http://dx.doi.org/10.33093/jetap.2024.6.1.5
8. Nagar N, Devra V. Green synthesis and characterization of copper nanoparticles using *Azadirachta indica* leaves. Mater Chem Phys. 2018;213: 44-51. http://dx.doi.org/10.1016/j.matchemphys.2018.04.007
9. Singh H, Desimone MF, Pandya S, Jasani S, George N, Adnan M, Aldarhami A, Bazaid AS, Alderhami SA. Revisiting the Green Synthesis of Nanoparticles: Uncovering Influences of Plant Extracts as Reducing Agents for Enhanced Synthesis Efficiency and Its Biomedical Applications. Int J Nanomed. 2023;18:4727-4750. http://dx.doi.org/10.2147/ijn.s419369
10. Yusnitati A, Anindita HN, Adha A, Septriana D., Priambodo TB, Hastuti ZD, Santoso E, Wulandari W, Zuldian P, Primeia S, Baruji T, Yurismono H, Prasetyo DH, Murti SDS, SendaSP, Saputra H. Biohydrogen production from palm oil mill effluent (POME) in Indonesia: Potential, challenges, and prospects. International Journal of Hydrogen Energy, 2025;138, 1315–1335. http://dx.doi.org/10.1016/j.ijhydene.2024.11.277
11. Mohamed JMM, Sivadasan D, Salawi A, Sultan MH, Muralidharan P, Venkatesan K, Asiri Y.I, Qushawy M, Pandurangam G, and Menaa F. A Novel Prednisolone-Loaded Layer-by-Layer Nanoparticles (LBL-NPs) for Rheumatoid Arthritis: Optimization and Therapeutic Evaluation. J. Pharm. Innov. 2025;20:124. https://doi.org/10.1007/s12247-025-10029-0
12. Moideen MMJ, Alqahtani A, Venkatesan K, Ahmad F, Krisharaju K, Gayasuddin M, Shaik RA. Application of the Box-Behnken design for the production of soluble curcumin: Skimmed milk powder inclusion complex for improving the treatment of colorectal cancer. Food Science & Nutrition 202;8(10):1-17. https://doi.org/10.1002/fsn3.1957
13. Al-Serwi RH, Eladl MA, El-Sherbiny M, Saleh MA, Othman G, Alshahrani SM, Alnefaie R, Jan AM, Alnasser SM, Aishah E. Albalawi AE, Mohamed JMM, Menaa F. Targeted Drug Administration onto Cancer Cells using Hyaluronic Acid-Quercetin Conjugated Silver Nanoparticles. Molecules 2023;28(10):4146. http://dx.doi.org/10.3390/molecules28104146
14. Chung A, Zaman N, Yaacof N, Yusoff N, Manaf S, Halim F, Majid R, Rusnani R. The Effectiveness of Gas Recovery Systems for Managing Odour from Conventional Effluent Treatment Ponds in Palm Oil Mills in Malaysia. Civil and Environmental Engineering Reports. 2019;29:70-85.: http://dx.doi.org/10.2478/ceer-2019-0025
15. Saputera WH, Amri AF, Mukti RR, Suendo V, Devianto H, Sasongko D. Photocatalytic Degradation of Palm Oil Mill Effluent (POME) Waste Using $BiVO_4$ Based Catalysts. Molecules. 2021;26(20):6225. https://doi.org/10.3390/molecules26206225
16. Jung B, Hoilat GJ. MacConkey Medium In: StatPearls Treasure Island (FL): StatPearls Publishing. 2025.
17. Tahir I, Amina SJ, Ahmed NM, Janjua HA. Antimicrobial coating of biologically synthesized silver nanoparticles on surgical fabric and surgical blade to prevent nosocomial infections. Heliyon. 2024;10(17):e35968. https://doi.org/10.1016/j.heliyon.2024.e35968

18. Thomas P, Sekhar AC, Upreti R, Mujawar MM, Pasha SS. Optimization of single plate-serial dilution spotting (SP-SDS) with sample anchoring as an assured method for bacterial and yeast cfu enumeration and single colony isolation from diverse samples. Biotechnol Rep (Amst). 2015;8:45-55. https://doi.org/10.1016/j.btre.2015.08.003

19. Klancnik A, Piskernik S, Jersek B, Mozina SS. Evaluation of diffusion and dilution methods to determine the antibacterial activity of plant extracts. J Microbiol Methods. 2010;81(2):121-126. https://doi.org/10.1016/j.mimet.2010.02.004

20. Unni V, Abishad P, Mohan B, Arya PR, Juliet S, John L, Vinod VK, Karthikeyan A, Kurkure NV, Barbuddhe SB, Rawool DB, Vergis J. Antibacterial and photocatalytic potential of piperine-derived zinc oxide nanoparticles against multi-drug-resistant non-typhoidal *Salmonella spp*. BMC Microbiol. 2025;25(1):89. https://doi.org/10.1186/s12866-025-03829-4

21. Amaliyah S, Pangesti DP, Masruri M, Sabarudin A, Sumitro SB. Green synthesis and characterization of copper nanoparticles using *Piper retrofractum Vahl* extract as bioreductor and capping agent. Heliyon. 2020;6(8):e04636. https://doi.org/10.1016/j.heliyon.2020.e04636

22. Nguyen TK, Thanh N Maclean S. Mahiddine Mechanisms of Nucleation and Growth of Nanoparticles in Solution. Chem Rev. 2014;114(15):7610–7630. https://doi.org/10.1021/cr400544s

23. Mohamed JM, Alqahtani A, Ahmad F, Krishnaraju V, Kalpana K. Pectin co-functionalized dual layered solid lipid nanoparticle made by soluble curcumin for the targeted potential treatment of colorectal cancer. Carbohydr Polym. 2021; 252:117180. https://doi.org/10.1016/j.carbpol.2020.117180

24. Chaabane L, Trendafilova I. Plasmonic nanostructures for enhanced photocatalytic overall water splitting. iScience. 2025;28(7):112799. https://doi.org/10.1021/acs.chemrev.4c00165

25. Nkosi NC, Basson AK, Ntombela ZG, Dlamini NG, Pullabhotla RVSR. Green Synthesis of Copper Nanoparticles Using a Bioflocculant from *Proteus mirabilis* AB 932526.1 for Wastewater Treatment and Antimicrobial Applications. Applied Nano. 2025;6:5. https://doi.org/10.3390/applnano6010005

26. García A, Rodríguez B, Giraldo H, Quintero Y, Quezada R, Hassan N, Estay H. Copper-Modified Polymeric Membranes for Water Treatment: A Comprehensive Review. Membranes (Basel). 2021;11(2):93. https://doi.org/10.3390/membranes11020093.

27. Abdelaziz AA, Kamer AMA, Al-Monofy KB, Al-Madboly LA. *Pseudomonas aeruginosa's* greenish-blue pigment pyocyanin: its production and biological activities. Microb Cell Fact. 2023;22(1):110. https://doi.org/10.1186/s12934-023-02122-1.

28. Huang M, Oppermann-Sanio FB, Steinbüchel A. Biochemical and molecular characterization of the Bacillus subtilis acetoin catabolic pathway. J Bacteriol. 1999;181(12):3837-41. https://doi.org/10.1128/JB.181.12.3837-3841.1999.

29. Dominic D, Baidurah S. Recent Developments in Biological Processing Technology for Palm Oil Mill Effluent Treatment—A Review. *Biology* 2022;11(4):525. https://doi.org/10.3390/biology11040525

30. Williams KF, Chioma DM and Nyema H. Screening of Lipase Producing Fungi Isolated from Palm Oil Mill Effluent Impacted Soil. South Asian J Res Microbiol. 2025;19:20-29. https://doi.org/10.9734/sajrm/2025/v19i8457

31. Thomas R, Hamat RA, Neela V. Extracellular enzyme profiling of *Stenotrophomonas maltophilia* clinical isolates. Virulence 2014;5(2):326-30. https://doi.org/10.4161/viru.27724

32. Todorova M, Kosateva A, Petrova V, Ranguelov B, Atanasova-Vladimirova S, Avdeev G, Stoycheva I, Pisareva E, Tomova A, Velkova L, Dolashki A, Dolashka P. Green Synthesis of Antibacterial CuO Nanoparticles Based on the Synergy Between *Cornu aspersum Snail Mucus* and Ascorbic Acid. Molecules 2025;30(2):291. https://doi.org/10.3390/molecules30020291

33. Ifijen IH, Awoyemi RF, Faderin E, Akobundu UU, Ajayi AS, Chukwu JU, Lekan OK, Asiriuwa OD, Maliki M, Ikhuoria EU. Protein-based nanoparticles for antimicrobial and cancer therapy: implications for public health. RSC Adv. 2025;5:14966–15016. https://doi.org/10.1039/D5RA01427A

34. Mammari N, Lamouroux E, Boudier A, Duval RE. Current Knowledge on the Oxidative-Stress-Mediated Antimicrobial Properties of Metal-Based Nanoparticles. Microorganisms. 2022;10(2):437. https://doi.org/10.3390/microorganisms10020437

35. Božić Cvijan B, KoraćJačić J, Bajčetić M. The Impact of Copper Ions on the Activity of Antibiotic Drugs. Molecules. 2023;28(13):5133. https://doi.org/10.3390/molecules28135133

36. Elfadadny A, Ragab RF, AlHarbi M, Badshah F, Ibáñez-Arancibia E, Farag A, Hendawy AO, De Los Ríos-Escalante PR, Aboubakr M, Zakai SA, Nageeb WM. Antimicrobial resistance of *Pseudomonas aeruginosa*: navigating clinical impacts, current resistance trends, and innovations in breaking therapies. Front Microbiol. 2024;15:1374466. https://doi.org/10.3389/fmicb.2024.1374466.

37. Ngece K, Khwaza V, Paca AM, Aderibigbe BA. The Antimicrobial Efficacy of Copper Complexes: A Review. Antibiotics (Basel). 2025;14(5):516. https://doi.org/10.3390/antibiotics14050516

38. Brooke JS. Advances in the Microbiology of *Stenotrophomonas maltophilia*. Clin Microbiol Rev. 2021;34(3):e0003019. https://doi.org/10.1128/CMR.00030-19.

39. Nalabothula R, Rani TS, Karthik BVS, Karra KR. Decoding the retroperitoneal mystery: a case of follicular lymphoma. Asian J. Pharm. Clin. Res. 2025;18(8):4-6. https://doi.org/10.22159/ajpcr.2025v18i8.55592

40. Tapan S, Pillai B. Phenolic and antioxidant alterations in wild edibles under different cooking methods. Int. J. Pharm. Pharm. Sci. 2025;17(10):15-22. https://doi.org/10.22159/ijpps.2025v17i10.55877

41. Muthu MJ, Kavitha K, Chitra KS, Nanthineeswari S. Soluble curcumin prepared using four different carriers by solid dispersions: Phase solubility, molecular modelling and physicochemical characterization. Trop J Pharm Res. 2019;18(8):1581. http://dx.doi.org/10.4314/tjpr.v18i8.21588Wylie MR, Merrell DS. The Antimicrobial Potential of the Neem Tree *Azadirachta indica*. Front Pharmacol. 2022;13:891535. http://dx.doi.org/10.3389/fphar.2022.891535.

42. Janczarek M, Endo M, Zhang D, Wang K, Kowalska E. Enhanced Photocatalytic and Antimicrobial Performance of Cuprous Oxide/Titania: The Effect of Titania Matrix. Materials 2018;11:2069. https://doi.org/10.3390/ma11112069

43. Mohamed JMM, Chinnaiyan S, Venkatesan K, Sivadasan D, Ahmad F, Al Oueslati MA, Ibraheem KM, ansal M, Goyal M, Nasreen A, Dineshkumar R. Optimization of polysaccharide extraction from *Mangifera indica* using response surface methodology and evaluation of its antioxidant activity. Colloid and Polymer Science 2025, 303:1577-1590. https://doi.org/10.1007/s00396-025-05431-6

Cite this article: Anu A, Krittika C, Sajna K P, Abiramy K, Maimuna G, Aishath A R, Soh L M, Nur I B T, Jamal M M M. Green-Synthesized Copper Nanoparticles from *Azadirachta Indica* for Antimicrobial Applications and Potential Visible-Light-Assisted Organic Load Reduction of POME. Pharmacogn J. 2026;18 (2): 129-138.